de Haas–van Alphen Effect and Fermi Surface in Rhenium*

A. S. Joseph and A. C. Thorsen
Atomics International Division of North America Aviation, Inc., Canoga Park, California
(Received 9 September 1963; revised manuscript received 8 November 1963)

The de Haas–van Alphen effect in rhenium has been studied by a null-deflection torsion balance technique in magnetic fields up to 40 kG. It is shown that a set of ellipsoids and a set of dumbbell-like Fermi surface segments located on the A–L symmetry line of the reduced Brillouin zone can account for most of the observed data. de Haas–van Alphen oscillations associated with magnetic breakdown phenomena provide evidence in support of the above model. This model furthermore requires that there be a degeneracy in the energy spectrum along the A–L line, as predicted by group theory.

I. INTRODUCTION

MEASUREMENTS of the de Haas–van Alphen effect, cyclotron resonance, magnetoacoustic absorption, magnetoresistance, etc., on nontransition metals have in general revealed that the Fermi surface of these metals can be well approximated by free-electron spheres with connectivity modifications at the electron Bragg reflection planes[1] (single orthogonalized-plane-wave approximation). The spheres are determined by the number of conduction electrons per unit cell, with the number of free electrons per atom assumed to be the same as the valence of the isolated atom. In the case of transition metals this assumption may not be valid. The free atom of rhenium for example has five electrons in the $5d$ band and two in the $6s$ band, and it is not clear *a priori* that these electrons should lose their identity in the solid to form a single Fermi surface as do the $3s^23p^1$ electrons in aluminum.[2] If they partially maintain their identity, the d-band and s-band electrons might have to be treated separately in the above approximation with an adjustable number of electrons in each band. Furthermore, the applicability of the single orthogonalized-plane-wave approximation may in itself be questionable in the case of transition metals.

Preliminary measurements by Thorsen and Berlincourt[3] have indicated that rhenium is rich in de Haas–van Alphen (dHvA) effect structure (periodic variation of the magnetic susceptibility with the reciprocal of the magnetic field) and it was believed that a detailed study of the orientation dependence of the periods of the dHvA oscillations might yield sufficient information to determine the Fermi surface. These periods P are directly related to the extremal cross-sectional areas (S) of the Fermi surface by the Onsager formula,[4]

$$P(\mathrm{G}^{-1})=2\pi e/\hbar cS=9.55\times10^{-9}/S(\text{Å}^{-2}).$$

In this paper we present the results of a systematic study of the dHvA effect in rhenium by means of the null-deflection torsion balance method. Although periods as low as 5×10^{-9} G^{-1} were detected they will be more accurately studied by pulsed-field methods and reported at a later date. A preliminary account of some of the novel multiple magnetic breakdown phenomena discovered in the course of this investigation has already been published.[5]

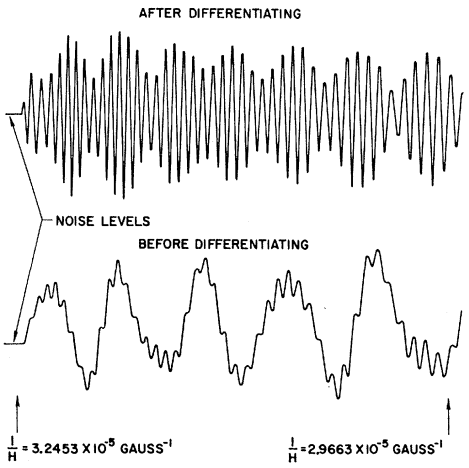

FIG. 1. Recording of de Haas–van Alphen oscillations before and after differentiation.

II. EXPERIMENTAL TECHNIQUES

The de Haas–van Alphen oscillations were observed by measurement of the torque exerted on a rhenium single crystal suspended in a steady magnetic field. A torsion balance similar to one described in an earlier report[6] was used with one important feature added. It was necessary to use a circuit that could record only the frequencies of interest because of the difficulty in analyzing the data when the torque contained several superimposed frequencies. The amplitudes of high-frequency terms were enhanced by a circuit which differentiated the signal from the torsion balance several times before it was recorded on a Moseley X-Y recorder. Figure 1 shows a typical sample of data recorded before and after differentiation. It is apparent that differentiating the signal considerably enhances the higher fre-

* Supported in part by the U. S. Atomic Energy Commission.
[1] *The Fermi Surface*, edited by W. A. Harrison and M. B. Webb (John Wiley & Sons, Inc., New York, 1960).
[2] W. A. Harrison, Phys. Rev. **116**, 555 (1959).
[3] A. C. Thorsen and T. G. Berlincourt, Phys. Rev. Letters **7**, 244 (1961).
[4] L. Onsager, Phil. Mag. **43**, 1006 (1952).
[5] A. S. Joseph and A. C. Thorsen, Phys. Rev. Letters **11**, 61 (1963).
[6] A. S. Joseph and W. L. Gordon, Phys. Rev. **126**, 489 (1962)

quency oscillations. With this modification periods as low as 5×10^{-9} G^{-1} could be observed.

Magnetic fields up to 40 kG were supplied by a 22-in. Varian V-3100 magnet and monitored to within 0.2% by a J. C. Carter probe and a Leeds and Northrup K-3 potentiometer which were calibrated by nuclear magnetic resonance and Rawson-Lush probes.

A rhenium rod purchased from the Chase Brass and Copper Company and zone refined in an electron beam furnace resulted in a residual resistivity ratio $[\rho(300°\text{K})/\rho(4.2°\text{K})]$ of 2700. Samples in the form of 0.09-in. diam by 0.15-in.-long cylinders were carefully spark cut along the $[1\bar{2}10]$, $[\bar{1}100]$, and [0001] directions. They were suspended in the magnetic field in five different orientations. In orientations 1, 2, and 3, the $[1\bar{2}10]$, $[\bar{1}100]$, and [0001] axes were parallel to the axis of suspension and hence the magnetic field was located in the $(1\bar{2}10)$, $(\bar{1}100)$, and (0001) planes, respectively. In all cases the [0001] axis was known to within 0.2° and axes in the basal plane were known to within 1.0°. Orientations 4 and 5 were similar to 1 and 2 except that in each case the [0001] was tilted 10° to 15° from the horizontal plane. The crystallographic directions are shown in the appropriate figures relative to the reduced Brillouin zone.

III. EXPERIMENTAL RESULTS AND DISCUSSION

A. Ellipsoids

The major portion of the de Haas–van Alphen terms observed in this study can be interpreted as resulting from two sets of closed segments of the Fermi surface. The longest period oscillations, arising from the set comprised of the smaller of the two segments, are labeled P_1 and shown in Figs. 2–4. Here the magnitude of the period is plotted versus θ and ϕ, where θ is the angle between the magnetic field and the [0001] axis, and ϕ is the angle from the $[10\bar{1}0]$ axis measured in the basal plane. The amplitudes of the P_1 oscillations are quite strong for most magnetic field directions. In Fig. 4, however, the lowest branch of P_1 disappears about 3° away from the $[11\bar{2}0]$ axis while in Fig. 3 the amplitudes of the oscillations of the lowest branch are very small and could be measured only through the region indicated by the solid line.

In Fig. 5, $P_1^2(\theta,\phi)$ is plotted versus $\cos^2(\theta,\phi)$ for sample orientations 1, 2, and 3. For each case, nearly a linear relationship is obtained, indicating that the Fermi surface segments responsible for P_1 are nearly ellipsoidal. In Table I, effective masses associated with P_1 are listed for several values of θ in the $(\bar{1}100)$ plane. These masses were calculated from the temperature dependence of the amplitudes of the dHvA oscillations.[7] For an ellipsoidal segment of the Fermi surface, the theory

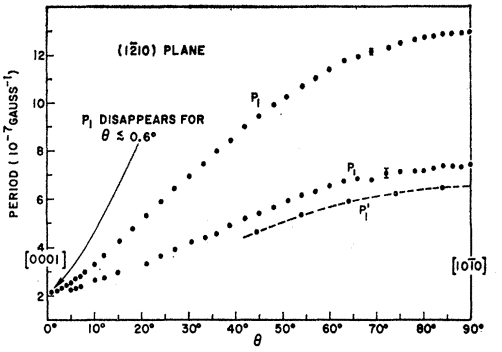

FIG. 2. dHvA periods P_1 and P_1' versus θ in the $(1\bar{2}10)$ plane.

of Lifshitz and Kosevich[8] requires that the product of the period and corresponding effective mass should be constant. The products of P_1 and $m^*(P_1)$, also shown in Table I, are seen to be approximately constant for $20°\lesssim\theta\lesssim80°$ but deviate considerably for smaller values

TABLE I. Effective masses and their product with P_1 are listed for various values of θ in the $(\bar{1}100)$ plane. Accuracy of effective mass values is estimated to be ±2%.

θ	$P_1\times10^7$ gauss^{-1}	m^*/m_0	$m^*/m_0\times P_1\times10^7$ gauss^{-1}
0	2.2	0.495	1.09
10	3.0	0.387	1.16
20	4.5	0.295	1.33
30	6.1	0.22	1.34
40	7.6	0.18	1.37
50	9.0	0.150	1.35
60	10.15	0.135	1.37
70	11.0	0.125	1.37
80	11.5	0.123	1.42

of θ. This suggests that the surfaces responsible for P_1 are not exactly ellipsoidal, even though a plot of P_1^2 versus $\cos^2\theta$ yields a straight line. Nevertheless, for simplicity we shall continue to refer to these segments as ellipsoids.

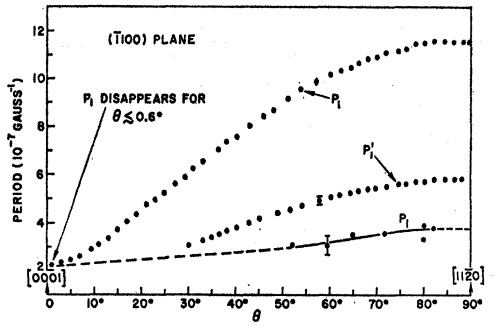

FIG. 3. dHvA periods P_1 and P_1' versus θ in the $(\bar{1}100)$ plane. In this plane two sets of ellipsoids should be observed. The lower curve of P_1 is very weak and could be seen only over a short range.

[7] D. Shoenberg, *Progress in Low Temperature Physics*, edited by C. J. Gorter (Interscience Publishers, Inc., New York, 1957), Vol. 2, pp. 226–65.

[8] I. M. Lifshitz and A. M. Kosevich, Zh. Eksperim. i Teor. Fiz. **29**, 730 (1955) [English transl.: Soviet Phys.—JETP **2**, 636 (1956)].

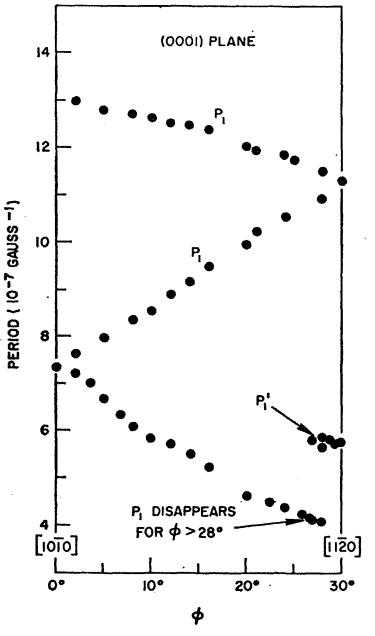

FIG. 4. dHvA periods P_1 and P_1' versus ϕ in the (0001) plane.

From the sixfold symmetry of P_1 in orientation 3 (Fig. 4), it follows that there are six of these ellipsoids situated in a plane parallel to or coincident with the hexagonal face of the reduced Brillouin zone with their major axes parallel to or along the A–L line. (The dashed lines of Figs. 3 and 4 are the extrapolated values of P_1 expected if the ellipsoids are situated as described.) For reasons to be discussed below we believe they are centered somewhere on the A–L line. Although the present data are not sufficient to determine the exact location of these segments on A–L, we tentatively place them as shown in Fig. 6(a), centered on the symmetry point L.

The periods corresponding to extremal areas of the ellipsoids along the [0001], [11$\bar{2}$0], and [10$\bar{1}$0] axes are 2.20×10^{-7}, 3.8×10^{-7}, and 1.30×10^{-6} G^{-1}, respectively. The corresponding areas in k space found from the Onsager relation are 4.34×10^{-2}, 2.5×10^{-2}, and 7.35×10^{-3} Å^{-2}. From these areas we calculate the axes of the ellipsoids to be $a=2.19\times10^{-1}$ Å^{-1} along [10$\bar{1}$0], $b=0.63\times10^{-1}$ Å^{-1} along [1$\bar{2}$10], and $c=0.366\times10^{-1}$ Å^{-1} along the [0001] direction.

The period labeled P_1' (Figs. 2–4), having a value of one half the corresponding value of P_1, is resolvable in the regions $45°<\theta<90°$ in the (1$\bar{2}$10) plane, $30°<\theta<90°$ in the ($\bar{1}$100) plane, and $25°<\phi<30°$ in the (0001) plane. The amplitude of P_1' is generally small in comparison to P_1 and is usually detected in the high field region just before the amplitude of P_2 and P_3 become large. In the (1$\bar{2}$10) and (0001) planes, P_1' is difficult to observe due to the presence of the lower branches of P_1, which have large amplitudes compared to P_1', and comparable periods. In the ($\bar{1}$100) plane P_1' is easily measured since the amplitude of the lower branch of P_1 is negligible. The effective masses $m^*(P_1')$ associated with P_1', and $m^*(P_1)$ associated with P_1 measured in the ($\bar{1}$100) plane are shown in Fig. 7. Within the accuracy of the experiment, $m^*(P_1')=2m^*(P_1)$ in agreement with the predictions of the Lifshitz-Kosevich theory for the pseudoeffective mass of the second harmonic. We thus associate the period P_1' with the second harmonic of P_1.

B. Dumbbells

The curves labeled P_2, P_3, and P_4 in Figs. 8–12 are attributed to the second set of Fermi surface segments. These segments resemble dumbbells in shape and can be thought of as two intersecting deformed spheres. From the symmetry of the curves we conclude that there are again six segments located in the same way as the ellipsoids discussed above. A sketch of one of these segments is tentatively centered on the point L as shown in Fig. 6(b), and approximate cross sections in the [11$\bar{2}$0] and [10$\bar{1}$0] directions are shown in Fig. 13(a), (b). (It should be noted that Fig. 1 in Ref. 5 should not have exhibited a waist for the dumbbell cross section in the [11$\bar{2}$0] direction.) With the magnetic field along the [0001] axis these surfaces exhibit two extremal areas. The period P_4 is attributed to the orbit labeled A in Fig. 6(b) while the orbit B through the waist of the dumbbell results in the periods P_2 and P_3. The A orbit decreases slowly in area as θ increases in the ($\bar{1}$100) and (1$\bar{2}$10) planes until the electron trajectory begins to cross the waist of the dumbbell. A further increase in θ is followed

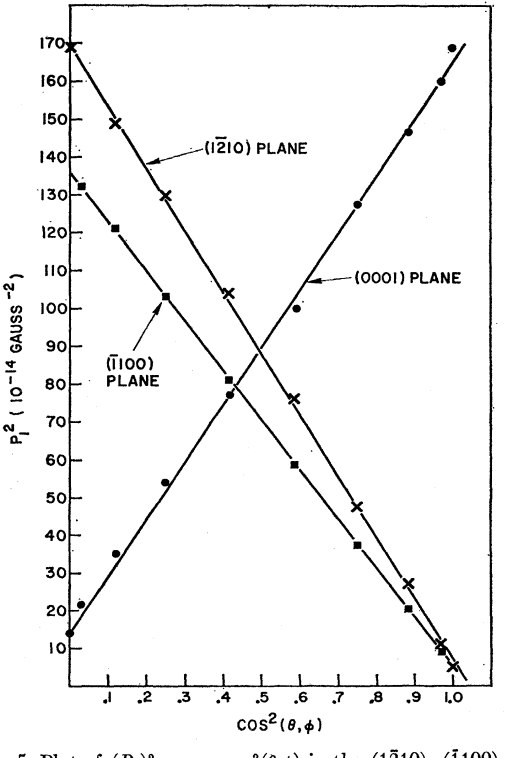

FIG. 5. Plot of $(P_1)^2$ versus $\cos^2(\theta,\phi)$ in the (1$\bar{2}$10), ($\bar{1}$100), and (0001) planes. The near linear relationships indicate that P_1 is due to a nearly ellipsoidal surface.

by an increase in the area until the orbit is no longer an extremal. This is in excellent qualitative agreement with the orientation dependence of P_4 (Fig. 8–9). In this region ($0°<\theta<28°$) the amplitudes of P_2 and P_3 are much larger than P_4 and hence no beats in P_4 are discernible. The existence or absence of beats in P_4 is indicative of the shape of the A orbit for the magnetic field near the [0001] direction. When the [0001] axis is tilted about 4° from the horizontal plane, beats in P_4 become apparent, thereby indicating that the A orbit is not circular. Figures 11 and 12 show the data for the [0001] axis tilted about 15° from the horizontal plane.

The rapid decrease of P_2 and P_3 away from the [0001] axis is a consequence of the fast increase in area of the B orbit as the magnetic field is rotated from the axis. (The apparent degeneracy of P_2 and P_3 in Fig. 9 is discussed in Sec. C.) At $\theta=45°$ P_2 has a broad minimum and begins to increase toward the basal plane. For $27°<\theta<60°$ the amplitude of P_2 is much smaller than that of P_3 such that the analysis of the former is somewhat inaccurate. (We should note that although P_2 and P_3 are a consequence of the same orbit they result from segments located at different positions in the reduced Brillouin zone.)

In the basal plane (Fig. 10) at least four frequencies of the same order of magnitude combine to give a complex pattern of long beats in the torque curves. Another period P_5 is seen to exist in this region and appears to approach P_2 at $\phi=0°$. The beats are so long, however, that it is not clear whether these two curves actually join. The analysis of the separate periods in this plane is extremely difficult since a miscount of one oscillation in seventy can shift a data point from one curve to another.

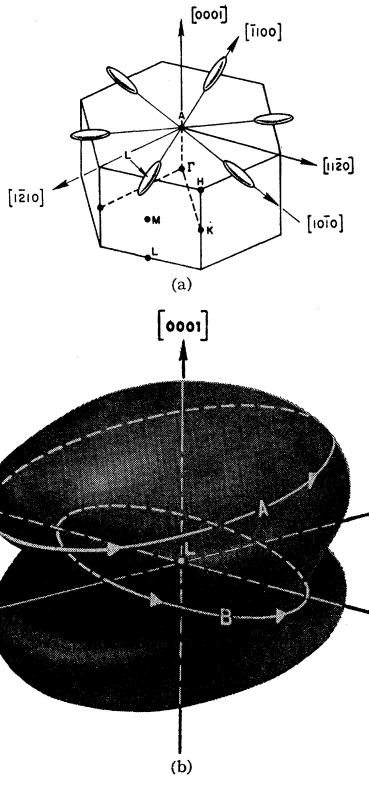

FIG. 6. (a) Possible location of ellipsoids in the reduced Brillouin zone. (b) Possible location of a dumbbell in the reduced Brillouin zone. These dumbbells are centered on the same points of the reduced zone as the ellipsoids. The orbit labeled A is responsible for P_4 and that labeled B is responsible for P_2 and P_3.

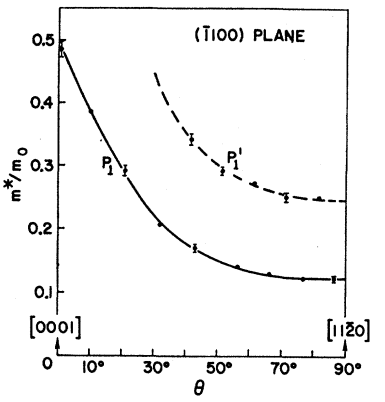

FIG. 7. Effective mass values of P_1 and P_1' in the (1̄100) plane. The pseudo-effective mass corresponding to the second harmonic of P_1 is denoted by the dashed curve.

The period P_5 and that labeled P_6 which is observed for $47°<\theta<53°$ in the (1̄100) plane cannot be assigned to a Fermi surface segment on the basis of the present data. The fact that they are observable only over a small range suggests that they result from orbits on a large section of the Fermi surface.

Effective mass values of the carriers responsible for the periods P_2, P_3, and P_4 at several orientations are given in Table II.

C. The A–L Degeneracy Line

Prior to the spin-orbit coupling calculations of Elliott[9] and Cohen and Falicov[10] it was thought that the hexagonal face of the reduced Brillouin zone in hcp metals was not an electron Bragg reflection plane. Inclusion of spin-orbit coupling in the band calculations shows the degeneracy in the energy spectrum along this face to be removed except along the symmetry line A–L. Consequently, barring magnetic breakdown, an electron incident on this plane will be Bragg reflected because of the spin orbit energy gap E_{SO} across the plane. However,

TABLE II. Effective masses of P_2, P_3, P_4, P_{12}, and P_{12}' in the (1̄100) plane. Accuracy of effective-mass values is estimated to be ±3% unless otherwise indicated.

θ	P_2	P_3	P_4	P_{12}	P_{12}'
0.4°	···	···	···	0.45	···
1.0°	···	0.47	0.62	···	···
15.0°	···	0.54	0.67±5%	···	···
30.0°	0.66	0.60	···	···	···
72.0°	0.73	···	···	···	···
88.7°	···	···	···	···	0.46

[9] R. J. Elliott, Phys. Rev. **96**, 280 (1954).

[10] M. Cohen and L. Falicov, Phys. Rev. Letters **5**, 544 (1960), and more recently L. Falicov and M. Cohen, Phys. Rev. **130**, 92 (1963).

reflection will not occur if the electron impinges along the A–L line where $E_{SO} \rightarrow 0$. Magnetic breakdown would occur if the energy gap $Eg \approx E_{SO}$ satisfied $Eg^2 < E_F\hbar\omega_c$,[11] where E_F = Fermi energy and ω_c is the cyclotron frequency. In transition metals with large atomic number however, one would expect the spin-orbit coupling and hence E_{SO} to be large so that in moderate magnetic fields $Eg^2 > E_F\hbar\omega_c$. It is likely, therefore, that magnetic breakdown effects would not be observed in the dHvA effect unless electron orbits cross the hexagonal face of the zone near the degeneracy line A–L, where $Eg^2/E_F\hbar\omega_c \rightarrow 0$.

In rhenium it appears that such a situation does occur. Both the ellipsoids and the dumbbells are required by the symmetry of the observed data to lie on a line parallel to or coincident with A–L. If we *assume* these segments are located on the A–L line a number of interesting observations can be made. When the magnetic field is in the neighborhood of the $[11\bar{2}0]$ axis, the extremal orbits on the two ellipsoids whose major axes are along the $[\bar{1}100]$ axis and the orbits on the corresponding dumbbells cross the hexagonal face of the reduced Brillouin zone in a region of near degeneracy (small spin-orbit splitting). Consequently, the probability is large that an electron would undergo a "magnetic breakdown." In this region around $\theta \approx 90°$ (Figs. 3 and 9) and $\phi \approx 30°$ (Figs. 4 and 10) the periods P_1 (lower branch) and P_2 resulting from the two ellipsoids and two dumbbells disappear and in their place a new period P_{12}' is observed (Figs. 9 and 10). In the transition region, $85° < \theta < 88°$, both P_1, P_2, and P_{12}' can be detected. This suggests a possible connection between the ellipsoid and the dumbbell segments. We note further that the extremal area corresponding to P_{12}' is exactly one-half the sum of the areas of the ellipsoid and dumbbell in this direction [i.e., $(P_{12}')^{-1} = (2P_1)^{-1} + (2P_2)^{-1}$]. Provided we assume that the two segments are both centered on the same point in the Brillouin zone, the period P_{12}' can be interpreted as a breakdown orbit between the ellipsoids and the corresponding dumbbell. For the field along the $[11\bar{2}0]$ axis the extremal cross-sectional

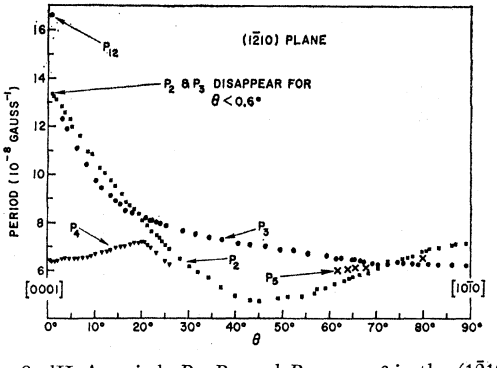

FIG. 8. dHvA periods P_2, P_3, and P_4 versus θ in the $(1\bar{2}10)$ plane. Note the occurrence of P_{12} near $\theta = 0°$.

[11] E. I. Blount, Phys. Rev. 126, 1636 (1962).

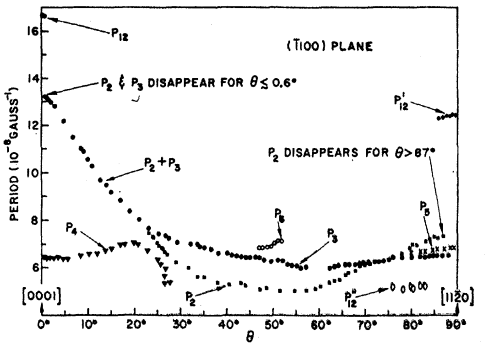

FIG. 9. dHvA periods P_2, P_3, P_4, P_5, and P_6 versus θ in the $(\bar{1}100)$ plane. Note the occurrence of P_{12} near $\theta = 0°$ and P_{12}' and P_{12}'' near $\theta = 90°$.

areas of the ellipsoids and dumbbells located on the $[\bar{1}100]$ axis are shown schematically in Fig. 13(c). If the energy gap between these segments becomes vanishingly small at points b and d [Fig. 13(c)], i.e., the A–L line is degenerate or nearly so, an electron could follow the path $bfghda$ [Fig. 13(d)] and lead to a dHvA period equal to that of P_{12}'. This period can be followed in the $(\bar{1}100)$ plane to about 5° from the $[11\bar{2}0]$ direction after which it rapidly disappears. The above model would predict such a disappearance since this breakdown orbit cannot be an extremal away from the $[11\bar{2}0]$ axis and still pass through the points b and d on the A–L line. In the (0001) plane P_{12}' disappears approximately 2° away from the $[11\bar{2}0]$ axis. According to this model, the orbits would then intersect the hexagonal face of the zone away from the A–L line where spin-orbit splitting becomes large. Farther from the

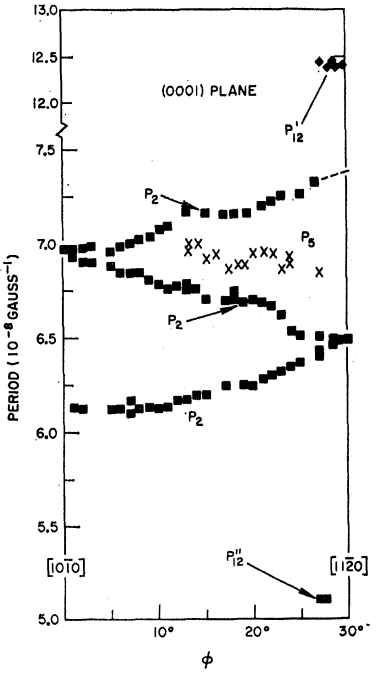

FIG. 10. dHvA periods P_2, P_3, P_5, P_{12}', and P_{12}'' versus ϕ in the (0001) plane.

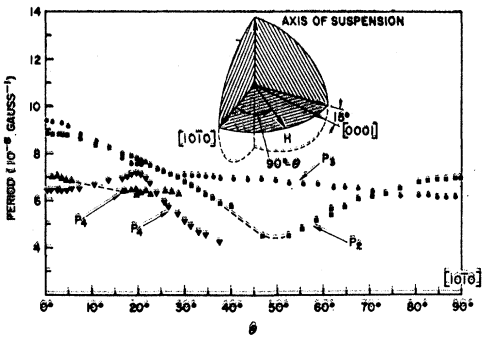

FIG. 11. dHvA periods P_2, P_3, and P_4 versus θ in a nonsymmetry plane. The [0001] was tilted about 15° from the horizontal plane. It is clear that P_4 has two components indicating that the A orbit is not circular about the [0001] axis. For $20°<\theta<27°$ the beat patterns in the torque curves are very complex.

[11$\bar{2}$0] axis we observe a weak period P_{12}'' which we associate with an orbit shown in Fig. 13(e). This corresponds to a situation of partial breakdown of the type discussed by Pippard.[12] The period is in accord with an area equal to the sum of the dumbbell area and twice the area of the ellipse and can be expressed as $(P_{12}'')^{-1}=(P_2)^{-1}+(P_1/2)^{-1}$. From Fig. 9 we find $P_1=38\times10^{-8}$ and $P_2=7.1\times10^{-8}$ G^{-1} at $\theta=72°$ from which we calculate $P_{12}''=5.1\times10^{-8}$ G^{-1}, in good agreement with the experimental value of 5.2×10^{-8} G^{-1}.

Along the [0001] axis, another composite orbit *kbfmhdk* [see Fig. 13(f)] might be expected to appear due to an energy degeneracy at points *b* and *d*. The period to be expected corresponds to an area of one-half the dumbbell waist plus one-half the ellipse, and hence is $(P_{12})^{-1}=(2P_1)^{-1}+(2P_2)^{-1}$. We calculate $(P_{12}=16.6\times10^{-8}$ G^{-1} as compared to the experimental period of 16.7×10^{-8} G^{-1} which can be observed over an angular range of approximately 0.6° (Figs. 8 and 9). Effective mass measurements of P_{12} and P_{12}' are listed in Table II.

Magnetic breakdown close to the A–L line would undoubtedly account for the vanishingly small amplitude of the lower branch of P_1 in the ($\bar{1}$100) plane and for its complete disappearance in the immediate neighborhood of the [11$\bar{2}$0] axis. All extremal orbits around the ellipsoid corresponding to this lower branch of P_1 would pass near or through the points *b* and *d* where the electrons could break through to another band and result in a diminution of the amplitude. Similarly, extremal orbits around the dumbbell giving rise to P_2 in the ($\bar{1}$100) plane would also pass near or through points *b* and *d*. As pointed out above the amplitude of the oscillations corresponding to P_2 was $\approx10\%$ that of P_3, except for $\theta\approx60°$ where P_3 passes through a minimum and its amplitude vanishes. For $79°<\theta<86°$ we observe the amplitude of P_2 to decrease in magnetic fields greater than 35 kG, becoming negligible at about 40 kG. This fact lends credence to the interpretation that the orbit responsible for P_2 does indeed experience magnetic breakdown. The amplitude of P_{12}'' in this region is also extremely small in comparison to P_3, reaching a maximum $\approx8\%$ of P_3 at $\theta\approx82°$.[13] P_{12}' is detectable near

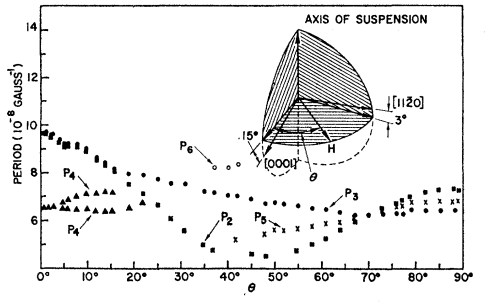

FIG. 12. dHvA periods P_2, P_3, P_4, P_5, and P_6 versus θ in a nonsymmetry plane. Here the [0001] and [11$\bar{2}$0] axes are tilted approximately 15° and 3°, respectively, from the horizontal plane.

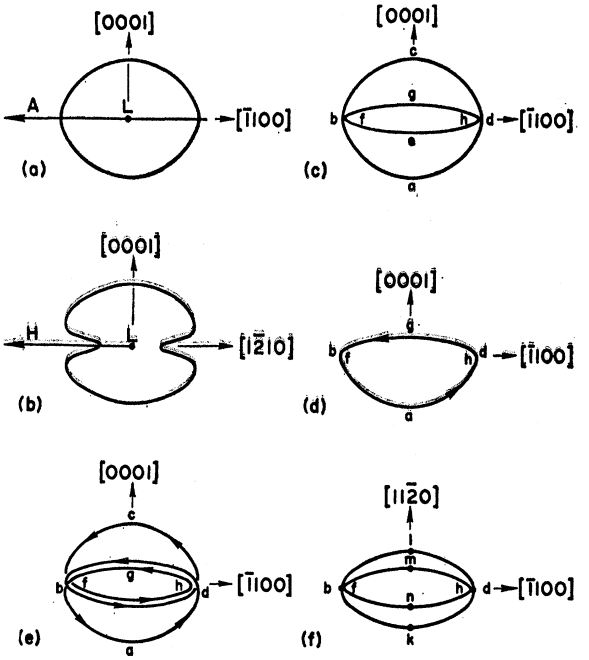

FIG. 13. (a) Approximate extremal cross section of the dumbbell in the (11$\bar{2}$0) plane. This area corresponds to the extrapolated value of $P_2=7.4\times10^{-8}$ G^{-1} (see Fig. 10). L and A are symmetry points in the reduced Brillouin zone. (b) Approximate cross section of the dumbbell in the (10$\bar{1}$0) plane. This area corresponds to a value of $P_2=6.2\times10^{-8}$ G^{-1} (see Fig. 10). H and L are the symmetry points in the reduced Brillouin zone. (c) Extremal cross sections of the ellipsoid and corresponding dumbbell in the (11$\bar{2}$0) plane, when the ellipsoid is placed within the dumbbell. (d) Orbit corresponding to complete magnetic breakdown between the ellipsoid and dumbbell in the (11$\bar{2}$0) plane, and accounting for P_{12}'. (e) Orbit corresponding to partial breakdown between the ellipsoid and dumbbell. Its path traces twice around the ellipsoid and once around the dumbbell and accounts for P_{12}''. (f) Extremal cross section of the ellipsoid and dumbbell in the (0001) plane. When θ is less than 0.6° the orbit *kbfmhdk* is observed. This orbit is responsible for P_{12}.

[12] A. B. Pippard, Proc. Roy. Soc. (London) **A270**, 1 (1962).

[13] We attribute the observation of P_1, P_2, and P_{12}'' in the ($\bar{1}$100) plane to slight misorientation of the sample. If the magnetic field could be accurately located in the ($\bar{1}$100) plane, electron

$\theta \approx 85°$ and its amplitude becomes larger than P_3 for $\theta > 87°$. Near the $[11\bar{2}0]$ axis the amplitude of P_{12}' shows a normal field dependence for a period of this magnitude, i.e., a gradual increase in amplitude with field.

In Fig. 9, P_2 and P_3 appear degenerate for $\theta < 22°$ in the $(\bar{1}100)$ plane. No beats were observed between P_2 and P_3 in this region even though at least 120 oscillations could be counted. It is of course possible that in this plane the pertinent dumbbells could result in identical periods in this angular range. However, an alternative explanation is that the amplitude of P_2 vanishes. According to the Lifshitz-Kosevich theory, the pth harmonic will vanish when the spin splitting factor, $\cos(p\pi m^*/m_0)$ in the expression for the amplitude of this harmonic is zero (m_0=free-electron mass). More recently, Cohen and Blount[14] have pointed out that when spin-orbit coupling is important the spin-splitting factor in the Lifshitz-Kosevich theory should be generalized to $\cos(p\pi m^*/m_s)$, where $m_s = 2m_0/g$ is the spin effective mass and g, the electron g factor, can differ appreciably from the value of 2. In Table II, the effective mass values of P_3 are listed for $\theta = 1°$ and 15°. If we assume that $m^*(P_3) \approx m^*(P_2) = 0.5m_0$ for $0° < \theta < 20°$ and $g = 2$ for the orbit associated with P_2, then the spin-splitting factor of P_2 will vanish. The assumption that $g = 2$ in this case is perhaps not unreasonable since for this orientation the electron orbit resulting in P_2 crosses the hexagonal face of the Brillouin zone near the line A–L where spin-orbit coupling is not important. The electron orbits associated with P_3 cross the Brillouin zone face 60° away from the A–L line where spin-orbit coupling is larger. This larger spin-orbit coupling could conceivably result in the g value differing from 2 to such an extent as to make the $\cos[\pi m^*(P_3)/m_s]$ term different from zero even though $m^*(P_3) \approx 0.5m_0$.

D. Single OPW Approximation

Models of the Fermi surface in the single orthogonalized-plane-wave (OPW) approximation[15] were constructed with free-electron spheres of adjustable volumes in an attempt to fit the observed data. Using spheres containing two to seven electrons per atom it was found that most of these models could not reasonably explain the experimental results without major modification of the various Fermi surface segments. They furthermore predicted many more dHvA oscillations than were actually observed. The model that comes closest to explaining the data is that resulting from spheres containing about 2 to 2.5 electrons per atom. The Fermi surface of this model would be similar to those of the beryllium series of the hcp metals when the single zone scheme[6] is used. For this case the overlaps in the fourth band and the "butterflies" of the third can with considerable modification qualitatively explain the periods P_1, P_2, P_3, P_{12}, P_{12}', and P_{12}''. However, the data give no evidence for the existence of the first band holes, the second band hole "monster," or the third band overlaps (needles), which are all or partially present in the low field dHvA oscillations in the hcp nontransition metals.

We might remark further that it is not possible to determine which band is responsible for the above surfaces. One can, however, use the single zone scheme in Harrison's[15] nearly free-electron model as a guide for labeling bands. Since the ellipsoids are located within the dumbbells, they would correspond to a higher band than the dumbbells if these segments are "electron" surfaces and vice versa if the segments are "hole" surfaces.

IV. CONCLUSIONS

The steady-field de Haas–van Alphen effect data can be interpreted as arising primarily from two sets of Fermi surface segments. The shape of the smaller sections is shown to be nearly ellipsoidal and the larger segments have a dumbbell-like shape similar to that resulting from two intersecting distorted spheres. The symmetry of the period versus orientation curves requires that both sets of segments be situated on lines parallel to the $\langle 10\bar{1}0 \rangle$ directions. The interpretation of the periods P_{12}, P_{12}', and P_{12}'' as breakdown orbits between the ellipsoids and the dumbbells requires that there be an energy degeneracy along these lines. Since the current band calculations provide no degeneracy line in the energy spectrum in these directions other than the A–L symmetry line, it can be concluded that the sections of Fermi surface are indeed situated on the A–L line. The existence of other periods (P_5 and P_6) over a small angular range suggests that these periods may be due to orbits on more complicated segments.

The segments of Fermi surface cannot be interpreted on the basis of a nearly free-electron model without considerable modification. A definite conclusion, however, should await high-field data on larger segments of the Fermi surface.

ACKNOWLEDGMENTS

The authors wish to thank Dr. T. G. Berlincourt, Dr. W. J. Tomasch, Dr. M. H. Cohen, Dr. R. E. Behringer, and Dr. T. Wolfram for valuable discussions and suggestions. We also wish to thank A. G. Presson and R. K. Seferian for making available the analog computers of the Applied Mathematics Unit for the analysis of the data, R. E. Gile for his assistance in taking the data, H. Nadler for growing the rhenium crystal, and D. Swarthout for orienting the crystals.

orbits would pass directly through the A–L line and complete breakdown would occur. In several runs when we believe the sample was more accurately oriented, the amplitudes of P_1, P_2, and P_{12}'' were much weaker and barely discernible.

[14] M. Cohen and E. I. Blount, Phil. Mag. 5, 115 (1960).

[15] W. A. Harrison, Phys. Rev. 118, 1190 (1960).

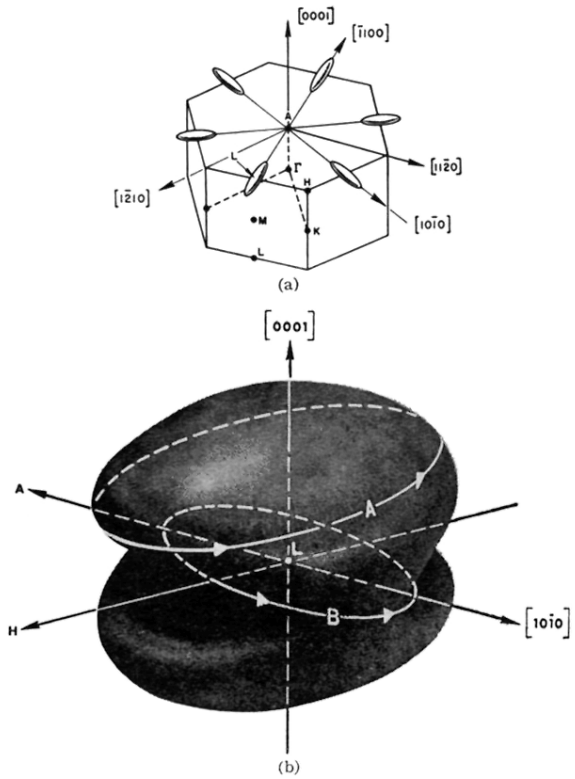

FIG. 6. (a) Possible location of ellipsoids in the reduced Brillouin zone. (b) Possible location of a dumbbell in the reduced Brillouin zone. These dumbbells are centered on the same points of the reduced zone as the ellipsoids. The orbit labeled A is responsible for P_4 and that labeled B is responsible for P_2 and P_3.